Geoinformation for European-wide Integration, Benes (ed.)

Object-based stem density estimates in a Mid-European forest district based on artifical neural nets – Comparison of Landsat-TM and HyMAP performances

C. Atzberger & M. Schlerf
Remote Sensing Department, University of Trier, Geozentrum, D-54286 Trier, Germany

Keywords: forest structure, stem density, hyperspectral, texture, artificial neural nets, image objects

ABSTRACT: Stem density is an important structural variable to be provided for the modelling of forest productivity. On a landscape scale its spatial distribution can only be mapped by remote sensing. However, the relation between stem density and forest reflectance is also affected by other confounding biophysical variables. Moreover, single pixels in high spatial resolution data may represent both illuminated and shaded tree crowns and also the underlying forest floor resulting in a highly variable surface reflectance.
We propose to avoid the negative effects of a highly variable spectral response through the use of objects covering a larger extent than single pixels. The use of objects is advantageous as textural features can be used as additional predictors at the same time. Reference data on stem density was automatically derived from black/white orthophotos (0.25 m resolution) by an algorithm which indentifies tree crowns and subsequently determines the number of trees per unit ground area. Various spectral and textural features have been extracted for each object from the hyperspectral data set and used to train artificial neural nets of varying network architectures. The trained neural nets were afterwards used to estimate stem densities of an completely independent test data set to validate the estimates. This approach allows us (i) to compare the performance of hyperspectral HyMAP imagery with (synthetic) Landsat-TM data and (ii) to evaluate the additional information content of several textural features.
Our results suggest that the estimation of stem density is feasible with a coefficient of determination (R^2) of about ≅0.6. The addition of textural features in the regression problem proved to be useful. The ill-posed nature of the regression problem has been identified to be responsible for this rather low accuracy. That is, different combinations of biophysical parameters may yield almost identical spectral signatures. Therefore, even artificial neural nets with many neurons in the hidden layer are not capable to identify object-based spectral / textural patterns solely related to stem density.

1 INTRODUCTION

1.1 *Remote sensing of structural variables*

Mapping of structural attributes is an important task in forest management and research, for instance modeling of forest productivity, carbon, water and nitrogen fluxes (Lucas & Curran, 1999; Waring & Running, 1999). Beside crown coverage and leaf area index (LAI), stem density and its intra-stand variability are also of importance (Cienciala et al., 1998; Curran, 1994; Korol et al., 1996).

Data from airborne and spaceborne sensors has been shown to provide much information for forestry applications (Franklin, 2001; Howard, 1991). The potential of remote sensing to derive stem density is supported by empirical studies (Atzberger & Schlerf, 2002b; Franco-Lopez et al., 2001) and through physically based reflectance modeling (Atzberger, 2000; Chen & Leblanc, 1997; Gastellu-Etchegorry et al., 1996; Kuusk & Nilson, 2000; Nilson & Peterson, 1991). However, one also has to notice the strong influence of other biophysical parameters on forest reflectance, such as leaf pigmentation, leaf water content, leaf area index, crown shape, understory reflectance, etc (Danson & Curran, 1993; Guyot et al., 1989). Moreover, different parameter combinations may form almost identical signatures. In summary, this leads to a highly variable, non-linear and "ill-posed" (Combal et al., 2001) relation between stem density and forest reflectance (Peterson, 1991; Wulder, 1998).

In the case of high spatial resolution data one also has to deal with the high spatial variability of the recorded signal, for example due to illuminated /shaded crowns and large gaps between the crowns. This effect can be avoided through the use of so-called image objects covering a larger extent than single pixels (Mäkelä & Pekkarinen, 2001; Wulder, 1998; de Kok et al., 1999; St-Onge & Cavayas,

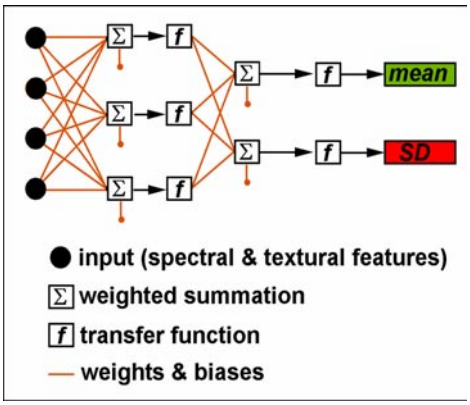

Figure 1. Schematic representation of a 4-3-2 artificial neural net with 4 input, 3 hidden and 2 output layers (per-field mean and standard deviation of stem density).

Figure 2. Study area "Idarwald" in the Western part of Germany. The area covered by the hyperspectral HyMAP image is approximately 10 x 4 km.

1997). The use of image objects is favourable, as textural measures can be used as additional predictors at the same time (Franklin et al., 2000; Muinonen et al., 2001; Wulder et al., 1998). Utilization of image objects is also mandatory when remotely sensed images are assimilated into ecological process models – mainly because of CPU limitations (Kimball et al., 2000).

1.2 *Neural networking*

Artificial neural networks (ANN) find more and more entry in remote sensing applications because they are able to (i) approximate functions, (ii) associate input vectors with specific output vectors, and (iii) classify input vectors in an appropriate way as defined by the user (e.g. Udelhoven et al., 2000; Berberoglu et al., 2000; Dawson et al., 1998; Gong et al., 1999; Rowland et al., 2001; Tatem et al., 2002).

Neural networks are composed of simple elements operating in parallel, with the network function being largely determined by the connections (weights) between the elements (Figure 1). The values of the connections between elements (i.e. weights and biases) are iteratively adjusted in a training step by presenting examples of proper network behavior to the network. This supervised training may require a large amount of computation time, especially when the training pattern set is large or many weights have to be adopted. But once training is completed, the appliance of the neural model on new data is very fast. A signal is propagated through a neuron of a multilayer network by just computing the scalar products of the input and the weight vectors. The result is then applied to a non-linear transfer function to generate the output (Figure 1).

1.3 *Objectives*

We decided to estimate stem density at the spatial resolution of image objects (i.e. forest stands) by means of artificial neural nets. The areal extent of the different image objects was determined using an existing Forest-GIS (Vohland, 1997).

The objectives of the study are (i) to compare the performance of hyperspectral HyMAP imagery with (synthetic) Landsat-TM data to estimate stem density, (ii) to evaluate the additional information content of textural information derived from the synthetic TM data, and (iii) to determine the optimum network architecture for this regression problem. The accuracies obtained in this study may also serve as a benchmark for results obtained through inversion of physically based forest reflectance models.

2 STUDY AREA

The area of study (49°40'N, 7°10'E) is located in the Idarwald forest in south-western Germany on the north-western slope of the Hunsrück mountain ridge (Figure 2). The dominant forest species are Norway spruce *(picea abies)*, beech *(fagus sylvatica)*, oak *(quercus petraea)* and Douglas fir *(pseudotsuga menziestii)*. Active forestry practices in this area include selective cutting, plantation establishment and thinning.

The most recent forest inventory for the study area (01.10.1994) including stand information on species composition, age classes etc. has been integrated into a Geographical Information System (Fo-GIS) by Vohland (1997). It is a very useful database to delineate the various forest stands, which serve as image objects.

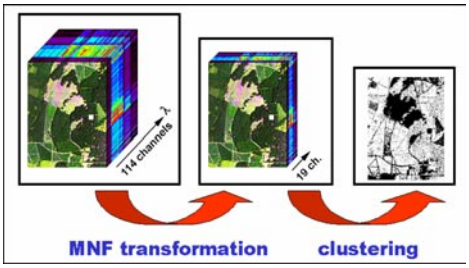

Figure 3. Applied methodology to generate a mask of conifers. The 114 channel HyMAP data cube is first reduced to 19 MNF fractions from which the mask is derived using the ISODATA algorithm.

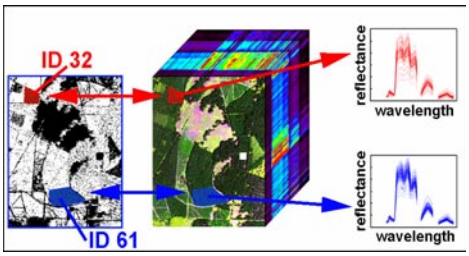

Figure 4. Illustration of the stand-wise extraction of HyMAP reflectances for two forest IDs which are used to calculate several spectral and textural features.

3 MATERIAL

Hyperspectral image data were acquired on 17 July 1999 with the HyMap sensor (Integrated Spectronics, Australia) mounted on board of an aircraft. HyMap records data in 128 contiguous spectral bands covering the spectral range of 0.4-2.5 µm with a spectral resolution of 10-20 nm. The spatial resolution was set to 5 m with a full scene covering approximately 4 km x 10 km. From the original image cube, 114 spectral bands with useful data have been selected through visual inspection.

Radiometric corrections of the HyMap data were performed using a modified 5S code (Tanré et al., 1981). The algorithm has been extended to take non-horizontal pixel orientation into account (Hill et al., 1995). Calibration constants of the sensor have been previously adjusted using own calibration targets. The dataset was geocoded using commerical available parametric image processing software PARGE (Schläpfer et al., 1998).

Twenty unstandardized black/white orthophotos (2 x 2 km) forming an image mosaic were used to determine the reference stem densities. The orthophotos (pixel size: 25 x 25 cm) derived from analogous photos of scale 1:5000 had been provided in digital form by the Landesvermessungsamt Rheinland-Pfalz, Germany.

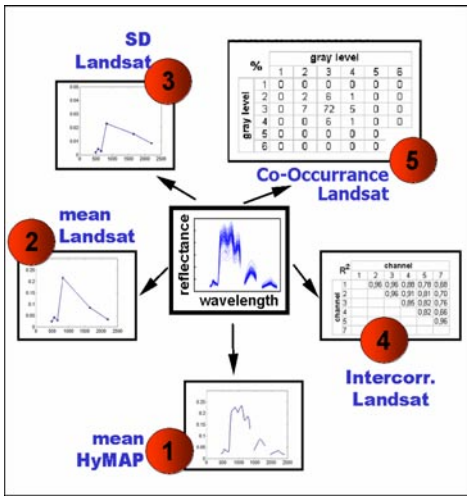

Figure 5. Utilization of stand-wise extracted HyMAP reflectances for calculation of several spectral and textural features.

4 METHODS

4.1 *Delineation of image objects*

Image objects were formed on the basis of the polygons representing the forest stands. Image pixels within a stand not representing conifers were excluded through masking. The mask of conifers had previously been build by an unsupervised classification (ISODATA algorithm) performed on the first 19 MNF-fractions of the HyMAP data cube (Schlerf et al., 2002) (Figure 3). All following calculations have been restricted to this mask. In this way, 150 forest stands of the Idarwald test region have been delineated and used for further analysis.

4.2 *Feature extraction*

For each of the 150 selected conifer stands, HyMAP reflectance curves were extracted for all pixels belonging to the conifer class (Figure 4). These spectral reflectances of each forest stand built the data base for the calculation of several object-based spectral – textural features (Table 1 and Figure 5). The first feature is simply the stand-wise mean of the HyMAP reflectances. The second and third feature are mean and standard deviation of spectral reflectances in TM channels, respectively. The fourth feature refers to the R^2 between spectral reflectances in TM channels. Since this matrix is symmetric, redundant entries have been removed. The last feature is the co-occurrence matrix of an 'albedo' image (inter-pixel sampling distance of one and zero degree angle). The albedo image is calculated as simply the mean of the TM reflectances. To obtain meaningful matrices, the albedo image has been recoded into 6 gray-levels, resulting in a gray-level co-occurrence matrix of size 6 x 6.

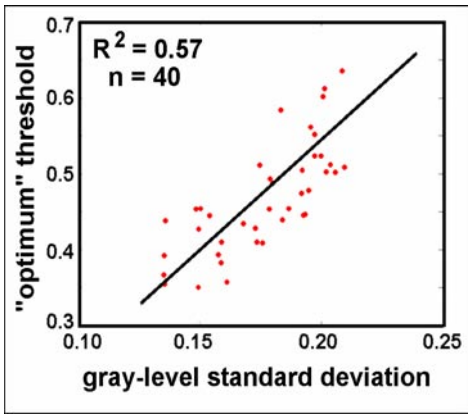

Figure 6. Experimentally obtained relation between the contrast of the black/white orthophotos (here standard deviation of the gray-levels in the 40 pictures analyzed) and the "optimum" threshold to be applied to allow for a separation between crowns and background. For further details refer to Atzberger & Schlerf (2002a)

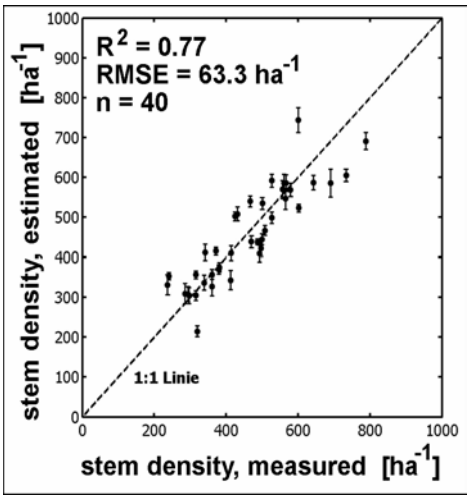

Figure 7. Observed versus estimated stem density. The statistics refer to cross-calibrated results.

4.3 *Reference stem densities*

A proper calibration of artificial neural nets requires large training samples. This is difficult to achieve through traditional ground sampling. We therefore developed an automatic method for processing of large mosaiks of black/white orthophotos (Atzberger & Schlerf, 2002a). In these orthophotos of high spatial resolution (25 x 25 cm), tree crowns are typically visible as almost distinct objects. Hence, the major task was to develop an algorithm which automatically separates crowns from the background and then identifies and counts the number of trees.

Analyzing the black/white orthophoto mosaic of the Idarwald region we found that the separation of crowns from background is neither possible using an unique threshold for the whole data set, nor it is always possible to find in the histograms (of the flying window) the "optimum" threshold which properly separates both populations (i.e. pixels belonging to crowns and to the background, respectively).

However, the analysis of 40 reference pictures revealed that the "optimum" threshold best separating crowns and background is linearly dependent on the contrast (here standard deviation of gray-level values) in the pictures analyzed (Figure 6). Therefore, to determine the stem density for the actual position of the flying window (size 25 x 25 m) one has first to determine the contrast from which the optimum threshold is calculated. After application of the appropriate threshold, the resulting binary image is submitted to a morpholoigcal opening (erosion followed by dilation) (The Mathworks, 2000) and the resulting objects (crowns) are identified and counted.

Cross-calibrated results show that stem density can be determined within ±65 trees ha^{-1} by the aforementioned approach for forest stands having stem densities between 200 and 800 trees per hectare (Figure 7) (Atzberger & Schlerf, 2002a). The resulting image of the Idarwald test site (25 x 25 m ground resolution) is shown in (Figure 8a). From this image, per-field mean and standard deviation of the reference stem densities have been calculated (Figure 8bc). Notice that mean and standard deviation of the reference stem density reveal a small interdependence (Figure 9).

4.4 *Neural networking*

To estimate per-field density and variability from spectral/textural features we decided to use feed-forward networks with one hidden layer of sigmoid neurons followed by an output layer on linear neurons (Figure 1). This kind of network can approximate any function with a finite number of discontinuities, arbitrarily well, given sufficient neurons in the hidden layer (Hagan et al., 1996). Properly trained back-propagation networks tend even to give reasonable answers when presented with inputs they have never seen. This generalization property makes it possible to train a network on a representative set of input/target pairs and get satisfying results without training the network on all possible input/output pairs.

One of the problems that occur during neural network training is called overfitting. The error on the training set is driven to a very small value, but when new data is presented to the network the error is large. The network has memorized the training

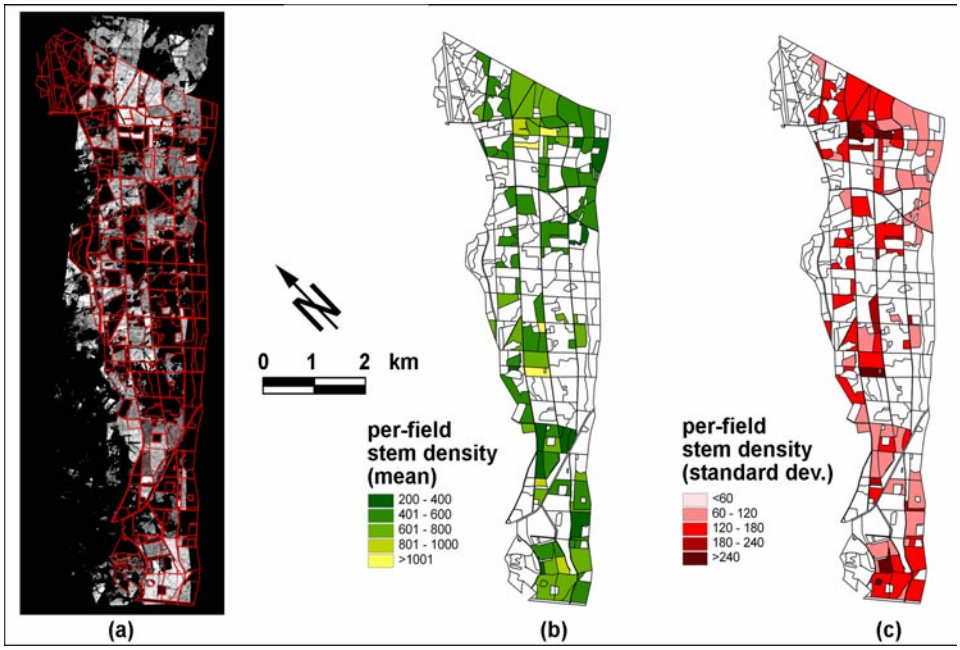

Figure 8. Reference stem densities obtained from black/white orthophotos using the algorithm developed by Atzberger & Schlerf (2002a). (a) pixel resolution, (b) per-field mean, (c) per-field standard deviation.

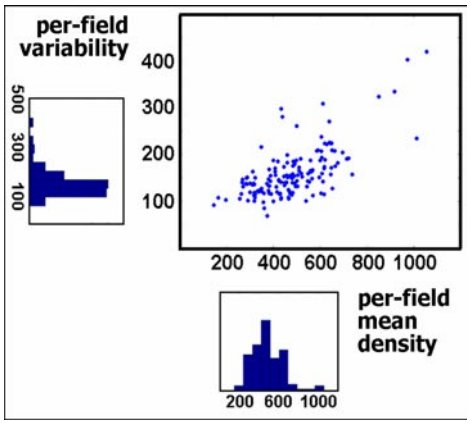

Figure 9. Interdependence between per-field mean density and per-field variability (SD) of the reference stem densities. Univariate histograms are also shown.

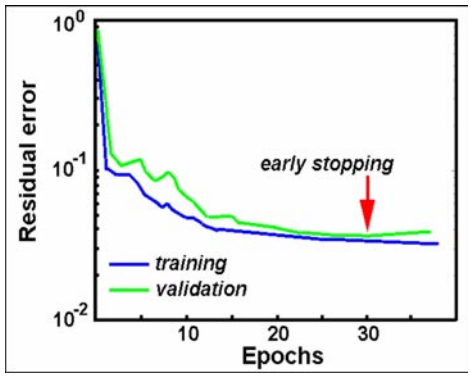

Figure 10. Illustration of the "early stopping" procedure. See text for further details.

examples, but it has not learned to generalize to new situations. To avoid overfitting, the data set (150 stands) has been divided into three subsets. The first subset is the training set (110 stands), which is used for computing the gradient and updating the network weights and biases. The second subset is the validation set (20 stands). The error on the validation set is monitored during the training process.

The validation error will normally decrease during the initial phase of training, as does the training set error (Figure 10). However, when the network begins to overfit the data, the error on the validation set will typically begin to rise. When the validation error increases for a specified number of iterations (here 10), the training is stopped, and the weights and biases at the minimum of the validation error are returned. These weights and biases are then used to estimate the dependent variables of the third data set: the test data set (20 stands). All statistics to be

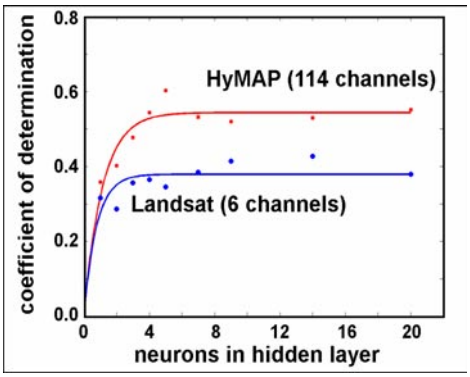

Figure 11. Coefficient of determination (R^2) between per-field reference densities and estimates as a function of the number of neurons in the hidden layer (i) for the 114 HyMAP channels as input vector, (ii) for the 6 TM channels as input.

Table 1. Description and resulting size of the 5 spectral and textural features used in this study. Note that the resulting size of the $TM_{intercorr}$ feature is 15 since from the original 6 x 6 matrix, diagonales and redundant entries have been removed. The 'albedo' image has been calculated as the mean over the 6 TM channels. The resulting floats have been afterwards recoded into 6 gray levels. See text for further details.

feature	description	size
HyMAP*mean*	mean spectral reflectance in HyMAP channels	1 x 114
TM *mean*	mean spectral reflectance in TM channels	1 x 6
TM *sd*	standard dev. of spectral reflectance in TM channels	1 x 6
TM *intercorr*	intercorrelation of spectral reflectance in TM channels	6 x 6 (*)
A*co-occ*	co-occurance (6 gray-levels) in albedo image	5+4+..1

(*) from the symmetric matrix, diagonale and redundant entries have been removed

shown in this contribution will solely report on this completely independent test data set.

From the many available training algorithms we chose the scaled conjugate gradient (SCG) which is known to perform well over a wide variety of problems (Moller, 1993). The SCG algorithm belongs to the family of conjugate gradient algorithms (The Mathworks, 2000). In the conjugate gradient algorithms a search is performed along conjugate directions, which produces generally faster convergence than the basic back-propagation algorithms which adjust the weights in the steepest descent direction (negative of the gradient).

The appropriate dimension of the hidden layer was found by comparing a range of models containing between 2 and 20 neurons. To avoid artefacts due to random initialization and to stabilize results, each neural net has been initialized 50 times. The reportet statistics (R^2) in this contribution refer always to the mean of these 50 repetitions.

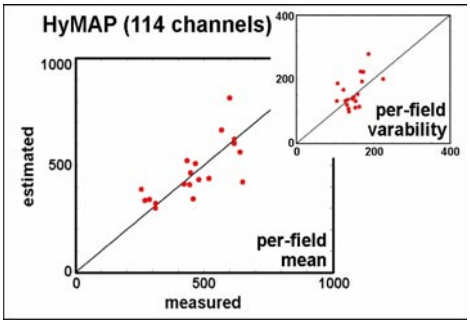

Figure 12. Measured versus estimated per-field density and variability using the 114 HyMAP channels as input (version 1).

Table 2. Coefficient of determination (R^2) between reference densities and estimates using neural nets (version 1 to 5) with 4 neurons in the hidden layer. Results are for the completely independent test data set (n=20) and calculated from 50 repetitions. 'Mean' refers to the per-field mean density and 'variability' to the per-field standard deviation of the stem density, respectively.

version	feature(s)	R^2 mean	R^2 variability
1	HyMAP*mean*	0.54	0.29
2	TM*mean*	0.36	0.30
3	TM*mean* + TM*sd*	0.62	0.31
4	TM*mean* + TM*intercorr*	0.48	0.25
5	TM*mean* + A*co-occ*	0.45	0.45

5 RESULTS & DISCUSSION

5.1 *Network architecture*

As expected, the coefficient of determination (R^2) between estimated and orthophoto derived stem density depends on the number of neurons in the hidden layer (Figure 11). However, R^2 begins to saturate at roughly 4 neurons in the hidden layer. This holds for all input variables (not shown). We therefore decided to further analyse only the neural nets with 4 neurons in the hidden layer. The different input parameters sets are summarized in (Table 1) and the corresponding results in (Table 2).

5.2 *Spectral dimension*

The degradation of the 114 channel HyMAP data set [version 1] (Figure 12) to a 6 channel TM data set [version 2] leads to a remarkable loss of prediction power (Figure 13). Apparently, the TM channels do not cover all spectral regions with useful information concerning stem density and its per-field variability.

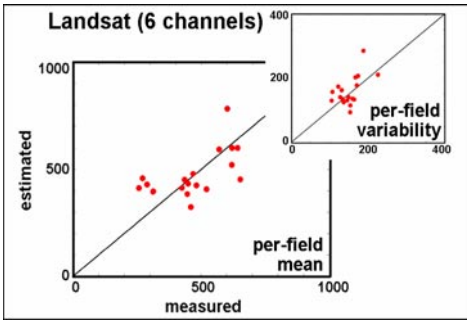

Figure 13. Measured versus estimated per-field density and variability using only the 6 TM channels as input (version 2).

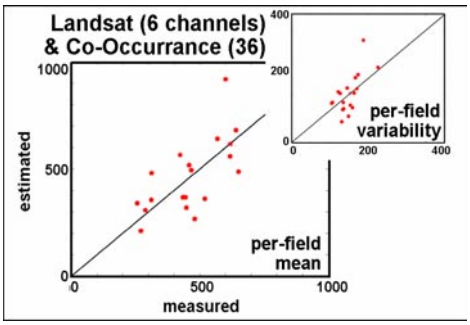

Figure 14. Measured versus estimated per-field density and variability using the 6 TM channels together with the co-occurance matrix as input (version 5).

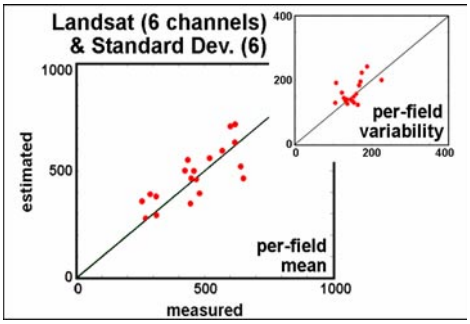

Figure 15. Measured versus estimated per-field density and variability using the 6 TM channels together with the 6 standard deviations as input (version 3).

5.3 *Textural information*

For a specified signal to noise ratio and image size one has to decide between a high spectral resolution (with a low spatial resolution) and a high spatial resolution (with a low spectral resolution). If the second option is preferred (i.e. high spatial resolution) one may additionally use the textural information as a further independent predictor.

Stem density and its intra-stand variability have been estimated using the spectral information of a Landsat TM sensor and the co-occurrence matrix derived from a 5 m "albedo" image [version 5] (Figure 14). Compared to the sole use of the TM spectral data [version 2] one observes an increase in prediction power. The achieved accuracies are comparable to those of the 114 channel HyMAP data set [version 1] (Figure 12). The results suggest that estimation of stem density does not necessitate the full spectral resolution of a hyperspectral imager as long as advantage is taken from the additional information provided by the co-occurrence matrix.

Since the calculation of co-occurrence matrices is time demanding we tested also a simpler textural measure based on standard deviations in TM channels [version 3]. The results obtained are as good as the previous ones (Figure 15). Obviously, in the case of 5 m resolution data, texture refers mostly to intra-field variability which is simply characterized by its standard deviation.

5.4 *Intercorrelation of spectral channels*

We tested also the intercorrelation of spectral (TM) channels as independent predictors [version 4]. Compared to the previously described textural features, no remarkable increase in prediction power could be observed (not shown). Therefore, in this form, the feature cannot be recommended.

6 CONCLUSION

In the present paper we tried to overcome the problems associated with a high spatial variability in the recorded signal through the use of so-called image objects. At the same time this offered the possibility to use textural measures as additional predictors.

The object-based approach of estimating stem density and its per-field variability gave promising results, but also confirmed known limits of remote sensing methods in forestry. Even neural nets with many neurons in the hidden layer were not able to estimate the per-field stem density with accuracies better than R^2=0.6. The explained variance was even worse when looking at the per-field variability of the stem density.

These findings confirm the ill-posed nature of the forest signature. That is, a given signature may be the result of different combinations of biophysical parameters. Therefore, no unique relation between the signature of an object and its stem density can be established. As far as structural variables are concerned, a stronger focus on multi-directional measurements seems inevitable (Chen et al., 2001; Sandmeier & Deering, 1999).

ACKNOWLEDGMENTS

This research was supported by the German Research Community (DFG) in the context of the interdisciplinary project "SFB 522: Umwelt und Region". The authors thank Joachim Hill (Trier) for the pre-processing of the HyMAP data. The Forest-GIS was provided by Michael Vohland and is gratefully acknowledged. The over-flight with the HyMap sensor was organized by Andreas Müller and Andrea Haushold of the German Aerospace Center (DLR). The Landesvermessungsamt Rheinland-Pfalz provided the black/white orthophotos used in the determination of reference stem densities.

REFERENCES

Atzberger (2000): Development of an invertible forest reflectance model: The INFOR-model.- *in: Buchroithner (Ed.): A decade of trans-european remote sensing cooperation. Proc. 20th EARSeL Symp. Dresden, Germany, 14-16 June 2000, 39-44*

Atzberger & Schlerf (2002a): Automatisierte Bestimmung der Bestockungsdichte in Nadelwäldern aus räumlich hochauflösenden Ortholuftbildern.- *in: Photogrammetrie, Fernerkundung, Geoinformation, 2002(3): 171-180*

Atzberger & Schlerf (2002b): Einsatz Neuronaler Netze zur empirischen Schätzung forstlicher Bestockungsdichten aus hyperspektralen Fernerkundungdaten.- *in: Müller, Monheim & Rumpf (Ed.): Umwelt und Region. Aus der Werkstatt des Sonderforschungsbereichs 522, Selbstverlag, Universität Trier, 197-206*

Berberoglu; Lloyd, Atkinson & Curran (2000): The integration of spectral and textural information using neural networks for land cover mapping in the Mediterranean.- *in: Computers & Geoscience, 26: 385-396*

Chen & Leblanc (1997): A four-scale bidirectional reflectance model based on canopy architecture.- *in: IEEE Trans. Geoscience and Remote Sensing, 35(5): 1316-1337*

Chen, Liu, Leblanc, Roujean & Lacaze (2001): Utility of multi-angle remote sensing for terrestrial carbon cycle modeling.- *in: Leroy (Ed.): 8th Intern. Symp. physical measurements and signatures in remote sensing. Aussois, France, Balkema, 249-260*

Cienciala, Running, Lindroth, Grelle & Ryan (1998): Analysis of carbon and water fluxes from the NOPEX boreal forest: Comparison of measurements with FOREST-BGC simulations.- *in: Journal of Hydrology, 62-78*

Combal, Baret, Poilvé & Polverin (2001): Using multispectral reflectance to retrieve LAI and chlorophyll content of Maize and Soybean.- *in: Leroy (Ed.): 8th Intern. Symp. physical measurements and signatures in remote sensing. Aussois, France, Balkema, 499-504*

Curran (1994): Attemps to drive ecosystem simulation models at local to regional scales.- *in: Foody & Curran (Ed.): Environmental remote sensing from regional to global scales. John Wiley & Sons, New York, 149-166*

Danson & Curran (1993): Factors affecting the remotely sensed response of coniferous forest plantations.- *in: RSE, 43: 55-65*

Dawson, Curran & Plummer (1998): The biochemical decomposition of slash pine needles from reflectance spectra using neural networks.- *in: IJRS, 19(7): 1433-1438*

de Kok, Schneider & Ammer (1999): Object-based classification and applications in the alpine forest environment.- *in: Int. Archives of Photogrammetry and Remote Sensing, Valladoloid, Spain*

Franco-Lopez, Ek & Bauer (2001): Estimation and mapping of forest stand density, volume, and cover type using the k-nearest neighbors method.- *in: RSE, 77: 251-274*

Franklin (2001): Remote sensing for sustainable forest management.- *Lewis Publishers, Boca Raton*

Franklin, Hall, Moskal, Maudie & Lavigne (2000): Incorporating texture into classification of forest species composition from airborne multispectral images.- *in: IJRS, 21(1): 61-79*

Gastellu-Etchegorry, Demarez, Pinel & Zagolski (1996): Modeling radiative transfer in heterogeneous 3-D vegetation canopies.- *in: RSE, 58: 131-156*

Gong, Wang & Liang (1999): Inverting a canopy reflectance model using neural network.- *in: IJRS, 20(1): 111-122*

Guyot et al. (1989): Factors affecting the spectral response of forest canopies: A review.- *in: GeoCarto Intern., 43-60*

Hagan, Demuth & Beale (1996) : Neural network design.- *PWS Publishing, Boston*

Hill.; Mehl & Radeloff (1995): Improved forest mapping by combining corrections of atmospheric and topographic effects.- *in: Askne (Ed.): Sensors and environmental applications of remote sensing, Proc. 14th EARSeL Symp., Göteborg, Sweden, 6-8 June 1994. A.A. Balkema, Rotterdam: 143-151*

Howard (1991): Remote sensing of forest resources. Theory and Application.- *Chapman & Hall, London*

Kimball, Keyser, Running, & Saatchi (2000): Regional assessment of boreal forest productivity using an ecological process model and remote sensing parameter maps.- *in: Tree Physiology, 761-775*

Korol, Milner & Running (1996): Testing a mechanistic model for predicting stand and tree growth.- *in: Forest Science, 42(2): 139-153*

Kuusk & Nilson (2000): A directional multispectral forest reflectance model.- *in: RSE, 72: 244-252*

Lucas & Curran (1999): Forest ecosystem simulation modelling: The role of remote sensing.- *in: Progress in Physical Geography, 23(3): 391-423*

Mäkelä & Pekkarinen (2001): Estimation of timber volume at the sample plot level by means of image segmentation and Landsat TM imagery.- *in: RSE, 77: 66-75*

Moller (1993): A scaled conjugate gradient algorithm for fast supervised learning.- *in: Neural Networks, 6: 525-533*

Muinonen, Maltamo, Hyppänen & Vainikainen (2001): Forest stand characteristics estimation using a most similar neighbor approach and image spatial structure information.- *in: RSE, 78: 223-228*

Nilson & Peterson (1991): A forest canopy reflectance model and a test case.- *in: RSE, 37: 131-142*

Peterson (1991): Applications in forest science and management.- *in: Asrar (Ed.): Theory and Applications of Optical Remote Sensing, 429-473*

Rowland, Danson, North & Plummer (2001): Comparison of neural network and LUT inversion techniques for retrieving forest LAI.- *in: Leroy (Ed.): 8th Intern. Symp. physical measurements and signatures in remote sensing. Aussois, France, Balkema, 507-512*

Sandmeier & Deering (1999): Structure analysis and classification of boreal forests using airborne hyperspectral BRDF data from ASAS.- *in: RSE, 69: 281-295*

Schläpfer; Schaepman & Itten (1998): PARGE: Parametric Geocoding Based on GCP- Calibrated Auxiliary Data.- *in: SPIE Int. Symp. on Opt. Sc, Eng. and Instr., San Diego: 334-344*

Schlerf, Atzberger & Hill (2002): Fernerkundliche Kartierung von Baumarten und Altersstufen unter Verwendung von Hyperspektraldaten und Ortholuftbildern.- *in: Müller, Monheim & Rumpf (Ed.): Umwelt und Region. Aus der*

Werkstatt des Sonderforschungsbereichs 522, Selbstverlag, Universität Trier, 175-182

St-Onge & Cavayas (1997): Automated forest structure mapping from high resolution imagery based on directional semivariogram estimates.- *in: RSE, 61: 82-95*

Tanré et al. (1981): Influence of the background contribution upon space measurements of ground reflectance.- *in: Applied Optics, 20(20): 3676-3684*

Tatem, Lewis, Atkinson & Nixon (2002): Super-resolution land cover pattern prediction using a Hopfield neural network.- *in: RSE, 79: 1-14*

The Mathworks (2000): Neural network toolbox for use with MATLAB.- *3 Apple Drive, Natick*

Udelhoven, Atzberger & Hill (2000): Retrieving structural and biochemical forest characteristics using artificial neural networks and physically based reflectance models.- *in: Buchroithner (Ed.): A decade of trans-european remote sensing cooperation. Proc. 20th EARSeL Symp. Dresden, Germany, 14-16 June 2000, 205-211*

Vohland (1997): Einsatz von Satellitenbilddaten (Landsat TM) zur Ableitung forstlicher Bestandsparameter und Waldschadensindikatoren.- *Master thesis, University of Trier*

Waring & Running (1999): Remote sensing requirements to drive ecosystem models at the landscape and regional scale.- *in: Tenhunen & Kabat (Ed.): Integration hydrology, ecosystem dynamics, and biogeochemistry in complex landscapes, John Wiley & Sons, New York, 23-38*

Wulder (1998): Optical remote-sensing techniques for the assessment of forest inventory and biophysical parameters.- *in: Progr. Phys. Geogr., 22(4): 449-476*

Wulder, Mike A.; LeDrew, Ellsworth F.; Franklin, Steven E.; Lavigne, Mike B. (1998): Aerial image texture information in the estimation of nothern deciduous and mixed wood forest leaf area index (LAI).- *in: RSE, 64: 64-76*